Supporting Information

Magnetically navigated and near-infrared programmable nanoinducers for co-activating pyroptosis and ferroptosis in antitumor immunotherapy

Shengze Lu,‡[a] Xiaopeng Hao,‡[b] Haidong Zhao,[c] Liangquan Yang,[d] Zhengyi Liu,[a] Hehua Cui,[a] Ningyue Yu,[e] Jingchao Li,*[e] Rujia Fan,*[f] Yang Yu*[a]

[a] *Department of Breast Surgery, Henan Provincial People's Hospital, Zhengzhou University People's Hospital, Henan University People's Hospital, Zhengzhou, Henan 450003, China. E-mail: yuyang6081@163.com (Y. Yu)*

[b] *Department of General Surgery, First Medical Center of Chinese PLA General Hospital, Beijing 100853, China)*

[c] *Department of Breast Oncology & Surgery, The Second Hospital of Dalian Medical University, Dalian, Liaoning 116023, China.*

[d] *Department of Breast Surgery, Maternity & Child care center of Qinhuangdao, Qinhuangdao, Hebei 066000, China.*

[e] *State Key Laboratory of Advanced Fiber Materials, College of Biological Science and Medical Engineering, Donghua University, Shanghai 201620, China. E-mail: jcli@dhu,edu,cn (J. Li)*

[f] *Department of Obstetrics and Gynecology, Henan Provincial People's Hospital, Zhengzhou University People's Hospital, Henan University People's Hospital, Zhengzhou, Henan 450003, China. E-mail: fanrujia1980@126.com (R. Fan)*

‡ These authors contributed equally to this work

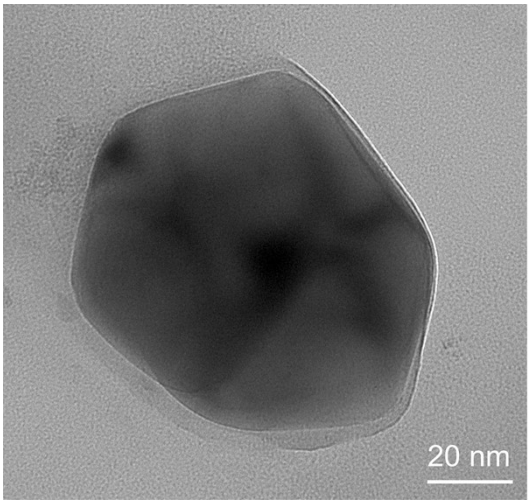

Fig. S1. Representative high-resolution TEM image of SP@CSFe (scale bar: 20 nm).

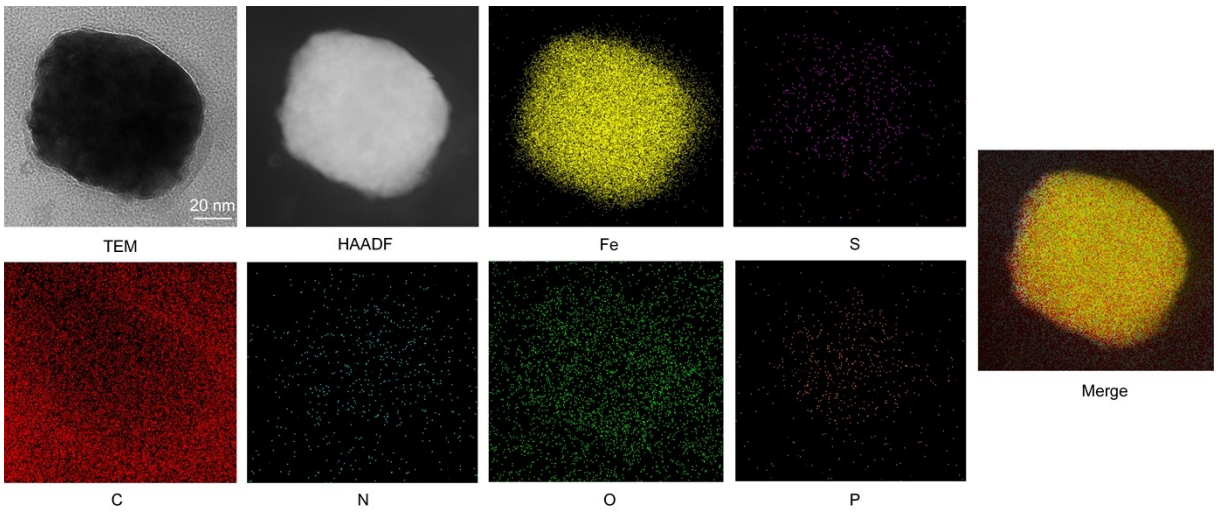

Fig. S2. Element mappings of SP@CSFe (Scale bar = 20 nm).

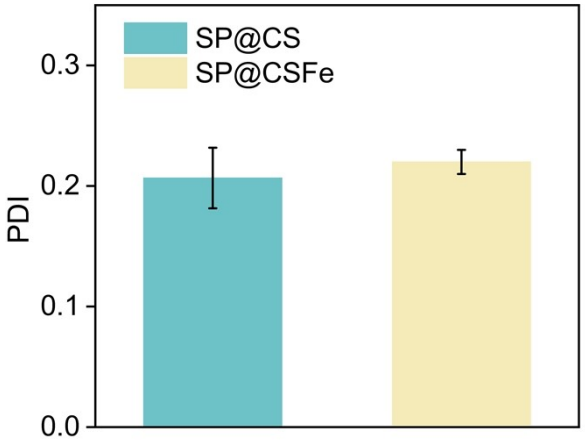

Fig. S3. Polydispersity index (PDI) of SP@CS and SP@CSFe (n = 3).

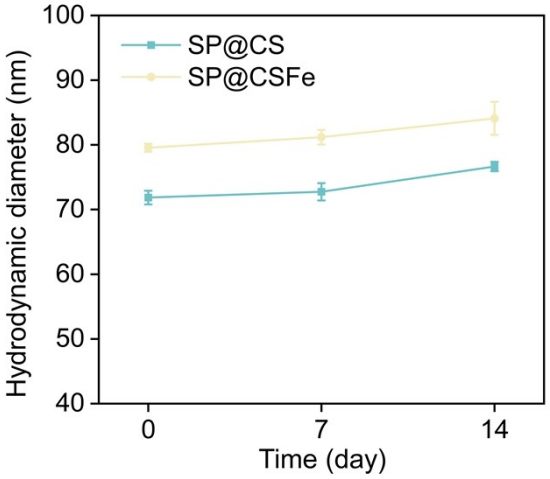

Fig. S4. Diameter stability of SP@CS and SP@CSFe monitored over 14 days in PBS at 4 ℃ (n = 3).

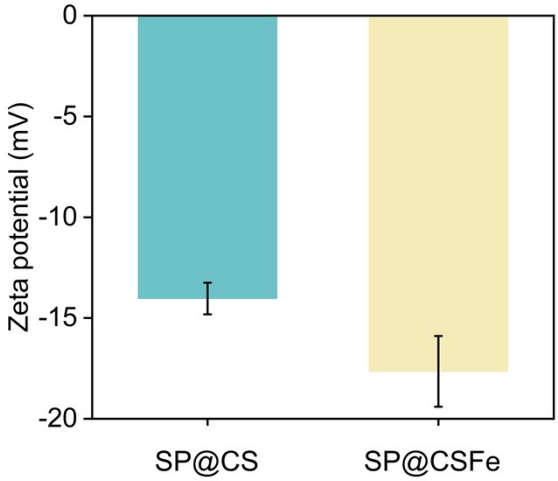

Fig. S5. Zeta potential values of SP@CS and SP@CSFe in FBS solusion (n = 3).

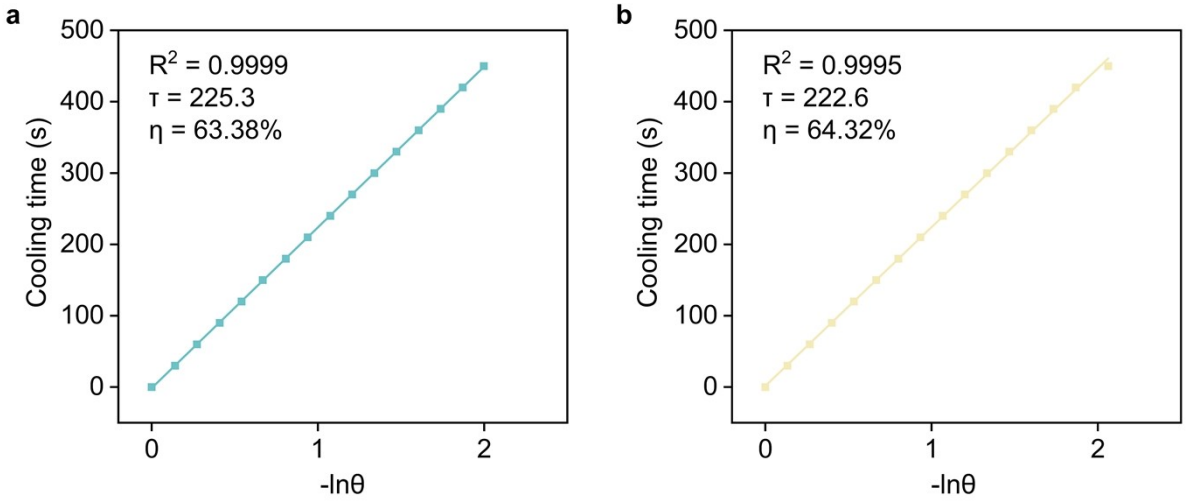

Fig. S6. The photothermal conversion efficiency of SP@CS and SP@CSFe.

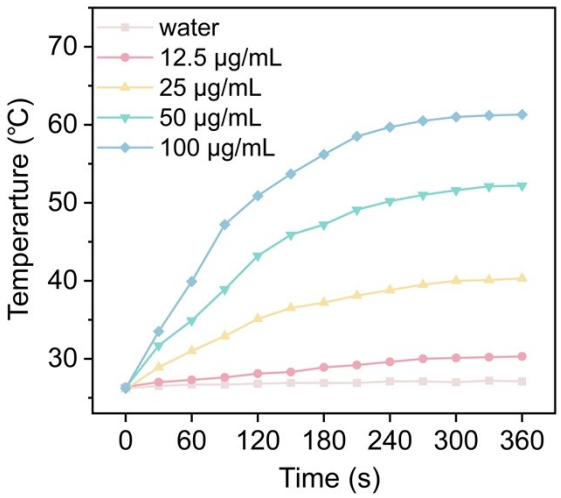

Fig. S7. Photothermal heating curves of SP@CS at different concentrations under 808 nm laser irradiation (1.0 W/cm^2).

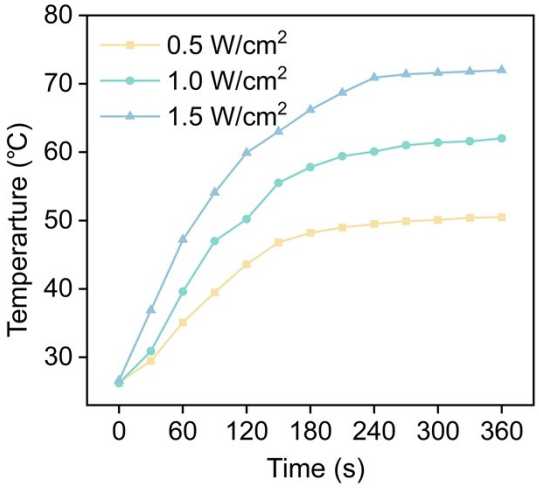

Fig. S8. Photothermal heating curves of SP@CS at different laser power densities (PCPDTBT: 100 μg/mL).

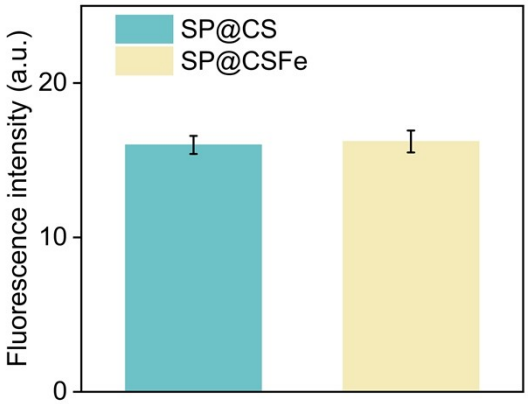

Fig. S9. Quantitative analysis of cellular uptake fluorescence intensity from CLSM images (n = 3).

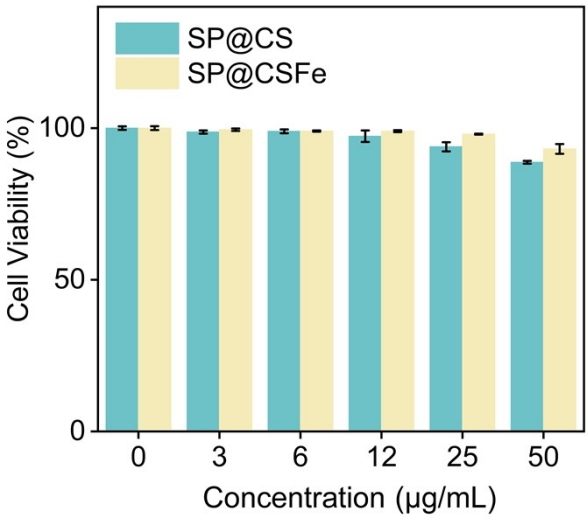

Fig. S10. Cytotoxicity of SP@CS and SP@CSFe in the absence of 808 nm laser irradiation (n = 5).

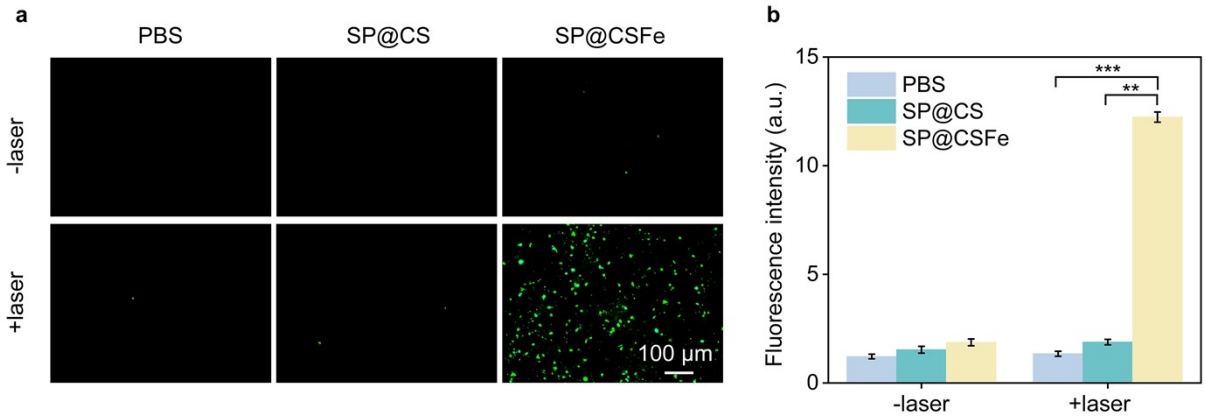

Fig. S11. (a) Representative fluorescence microscopy images of PBS, SP@CS and SP@CSFe group (scale bar: 100 μm). (b) Quantitative analysis of fluorescence intensity (n = 5).

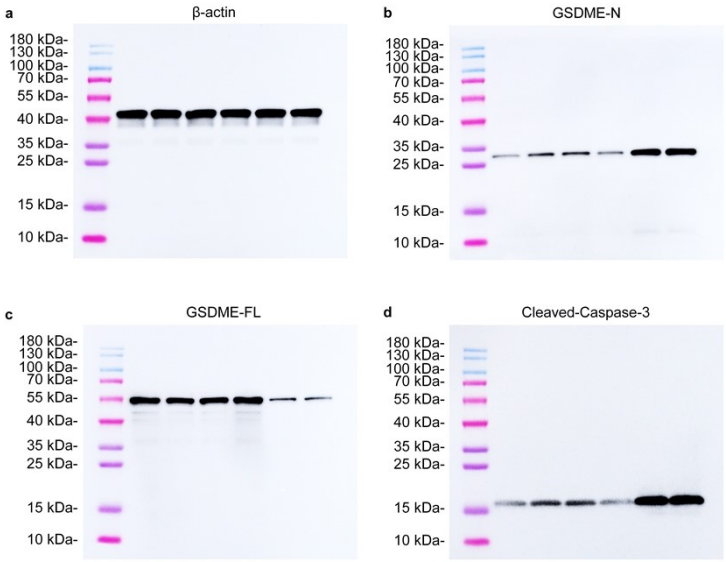

Fig. S12. Full, uncropped WB blots corresponding to Fig. 3e (pyroptosis markers).

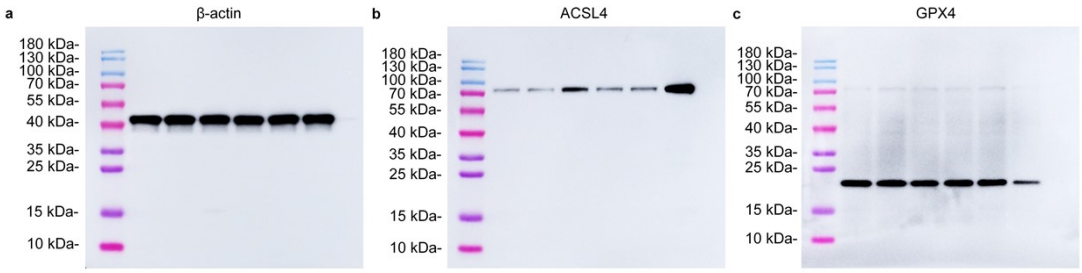

Fig. S13. Full, uncropped WB blots corresponding to Fig. 3g (ferroptosis markers).

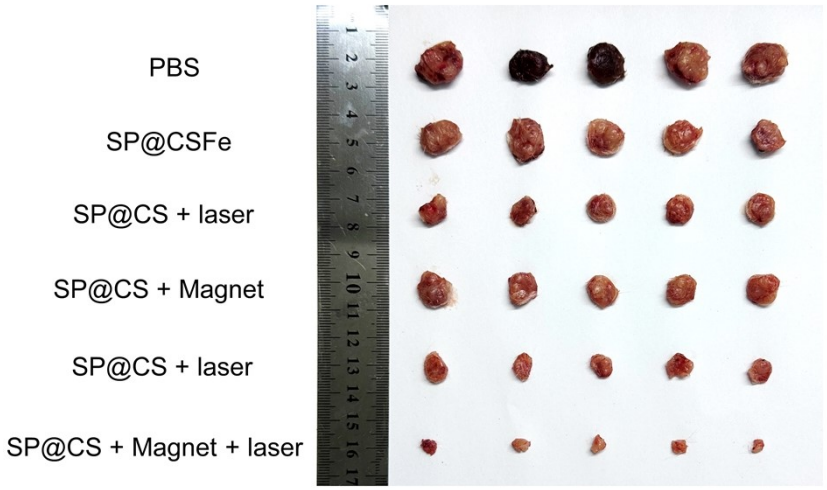

Fig. S14. Photographs of excised primary tumors from all groups on day 18 (n = 5).

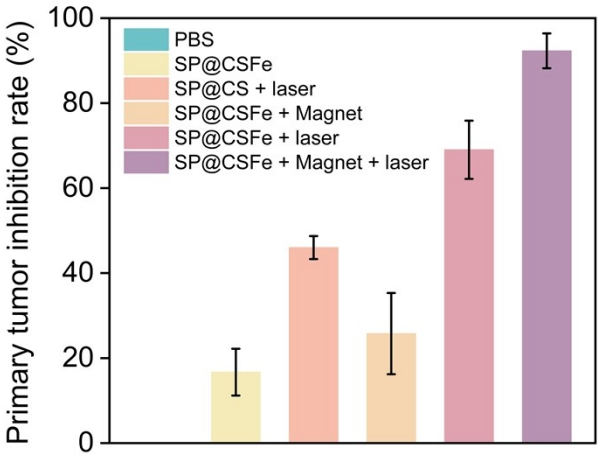

Fig. S15. Primary tumor inhibition rates calculated based on final tumor weights (n = 5).

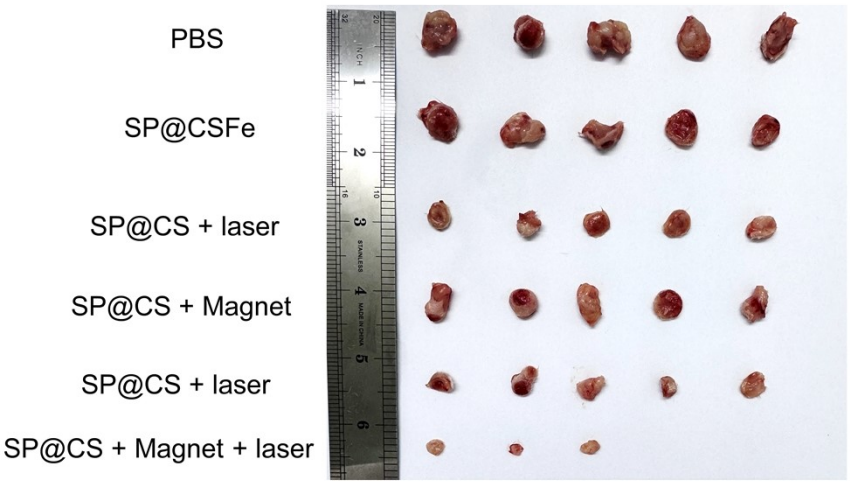

Fig. S16. Photographs of excised distant tumors from all groups on day 18 (n = 5).

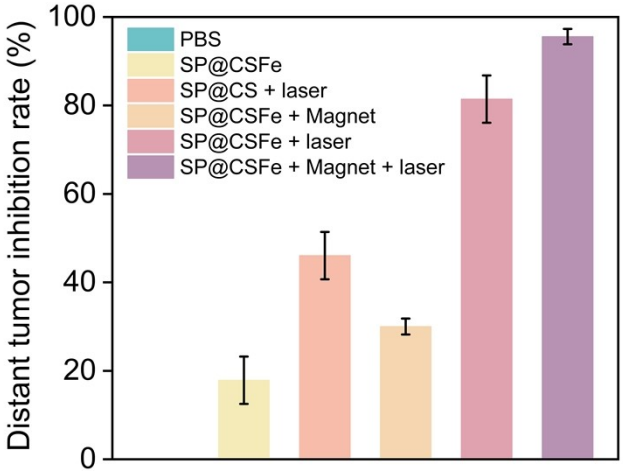

Fig. S17. Distant tumor inhibition rates calculated based on final tumor weights (n = 5).

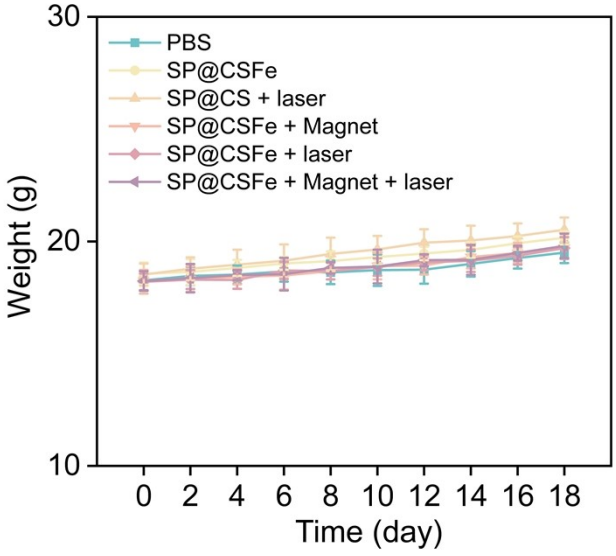

Fig. S18. Body weight changes of mice monitored over the 18-day treatment period (n = 5).

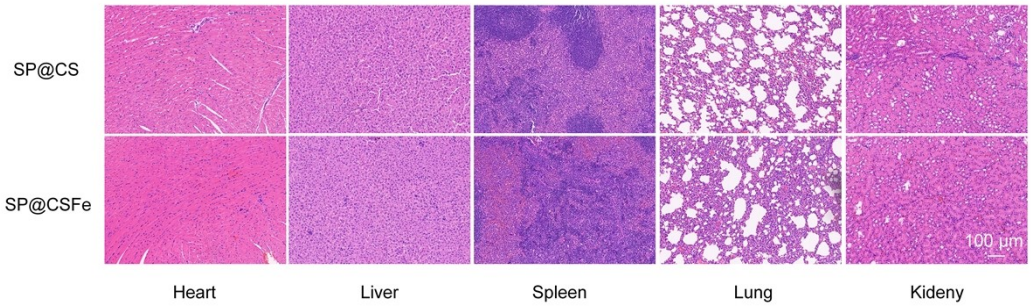

Fig. S19. H&E-stained sections of major organs from PBS-treated and SP@CSFe + Magnet + laser-treated mice (scale bar: 100 μm).

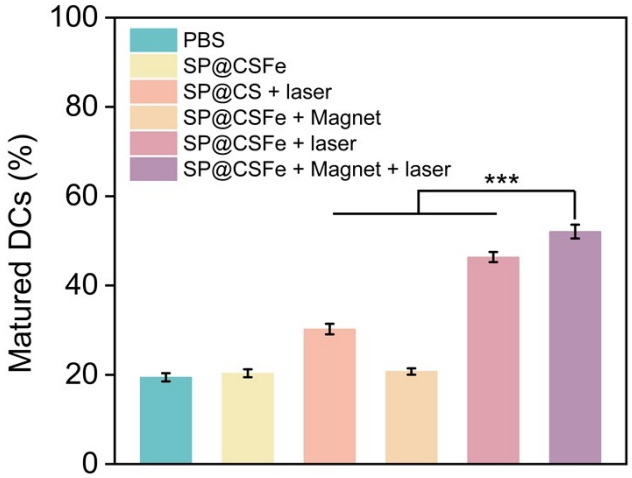

Fig. S20. Quantification of matured DCs ($CD80^+CD86^+$) in lymph nodes (n = 3).

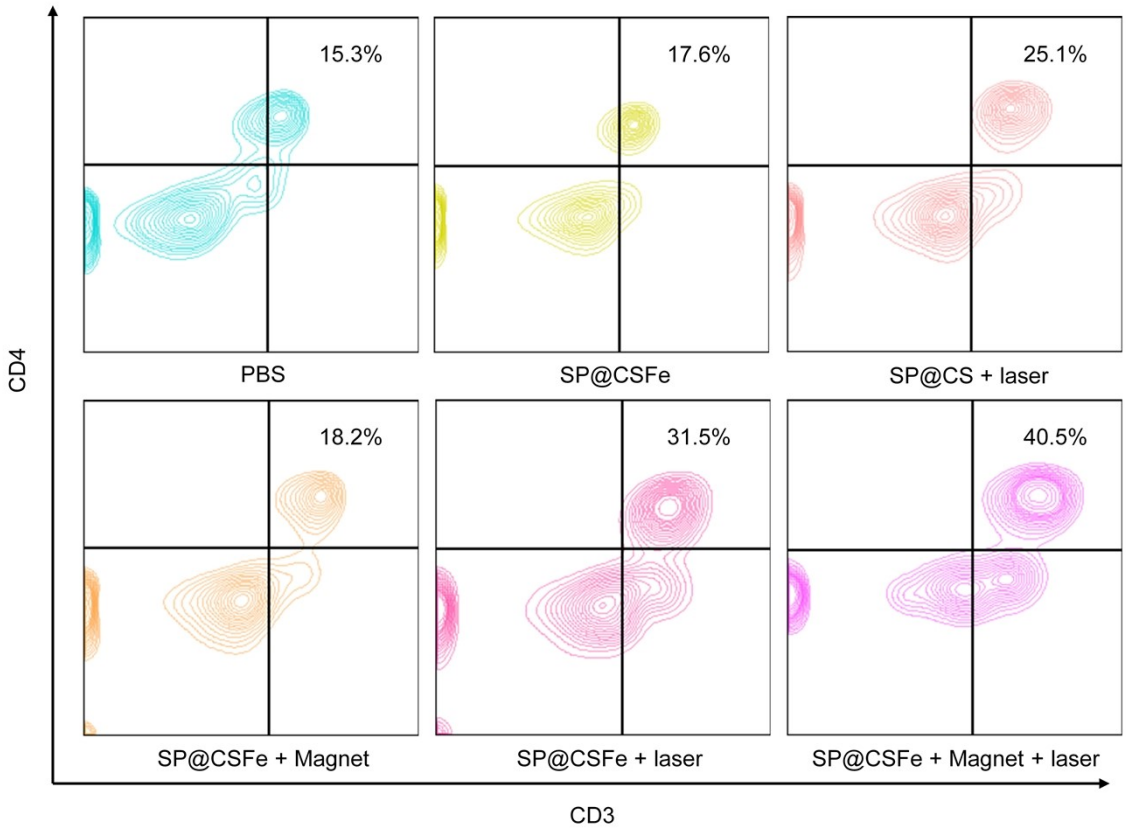

Fig. S21. Representative flow cytometry plots for $CD3^+CD4^+$ T cell analysis in primary tumors.

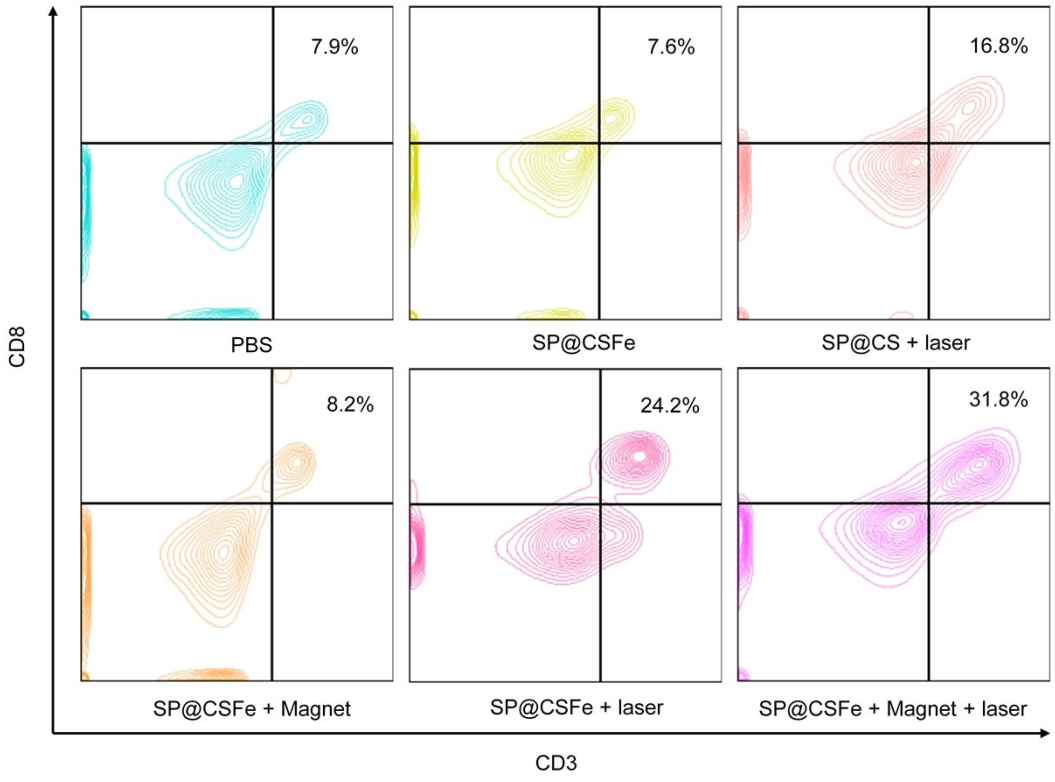

Fig. S22. Representative flow cytometry plots for $CD3^+CD8^+$ T cell analysis in primary tumors.

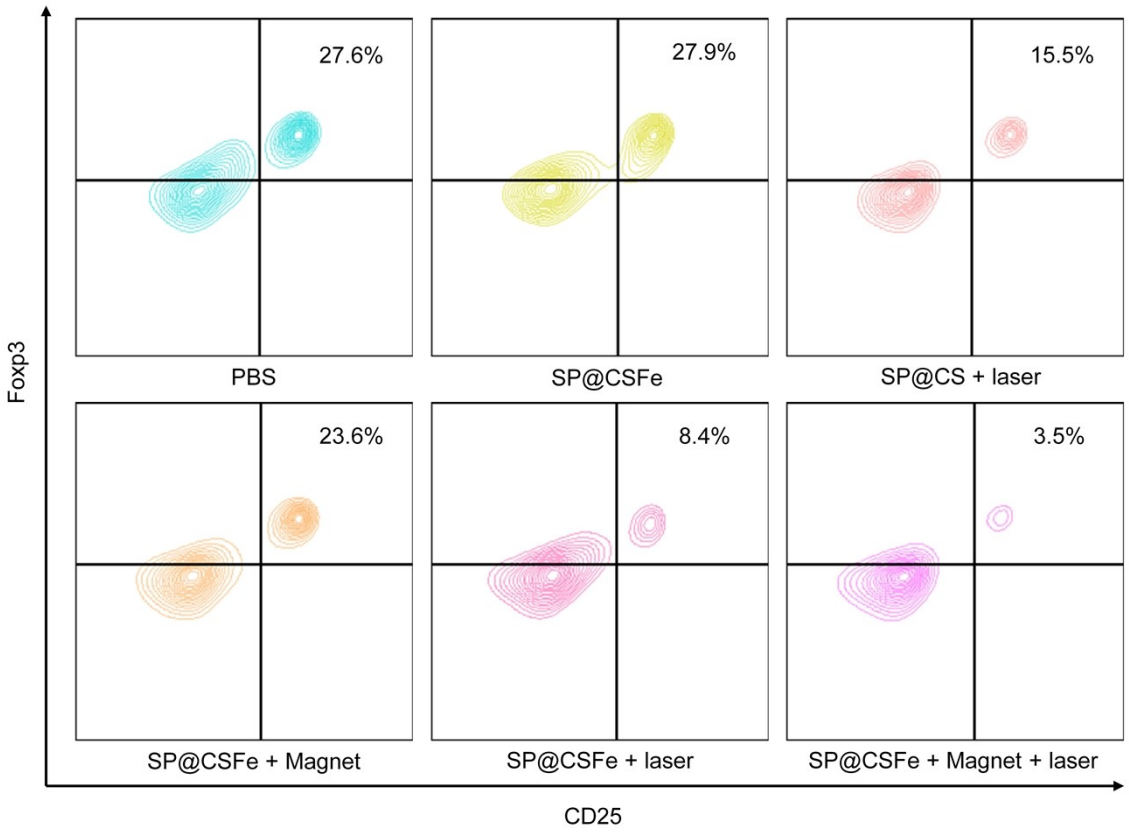

Fig. S23. Representative flow cytometry plots for T_{reg} ($CD25^+Foxp3^+$) cell analysis in primary tumors.

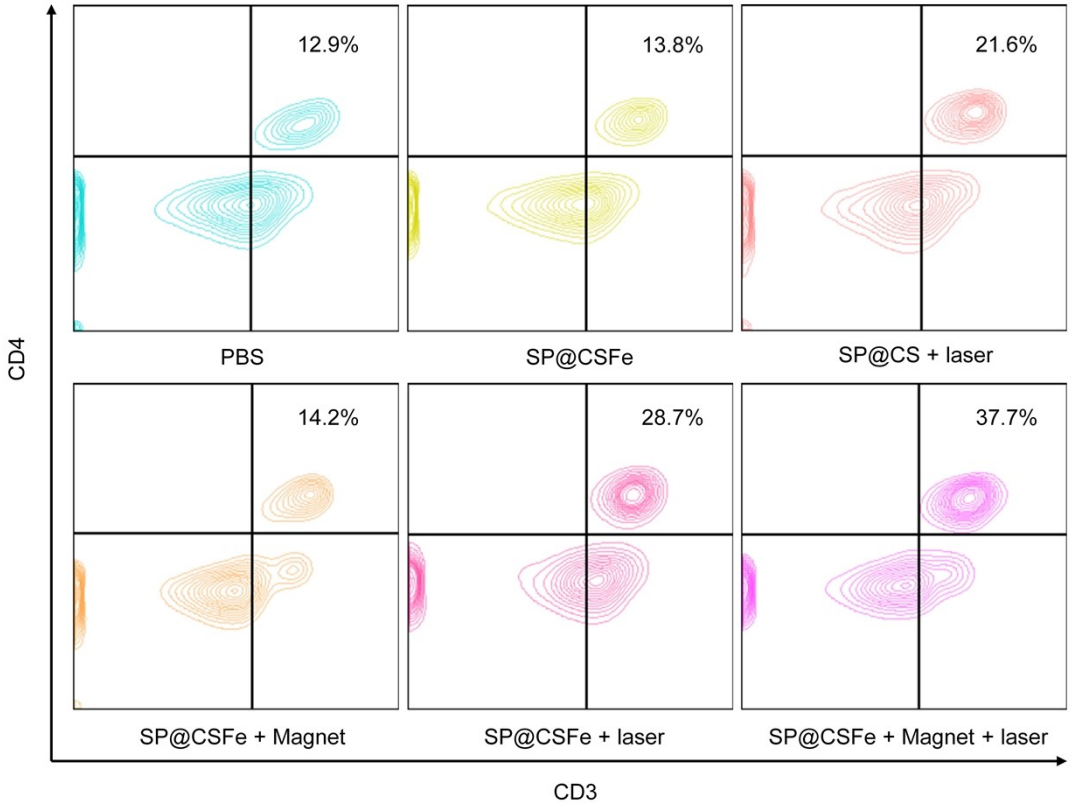

Fig. S24. Representative flow cytometry plots for $CD3^+CD4^+$ T cell analysis in distant tumors.

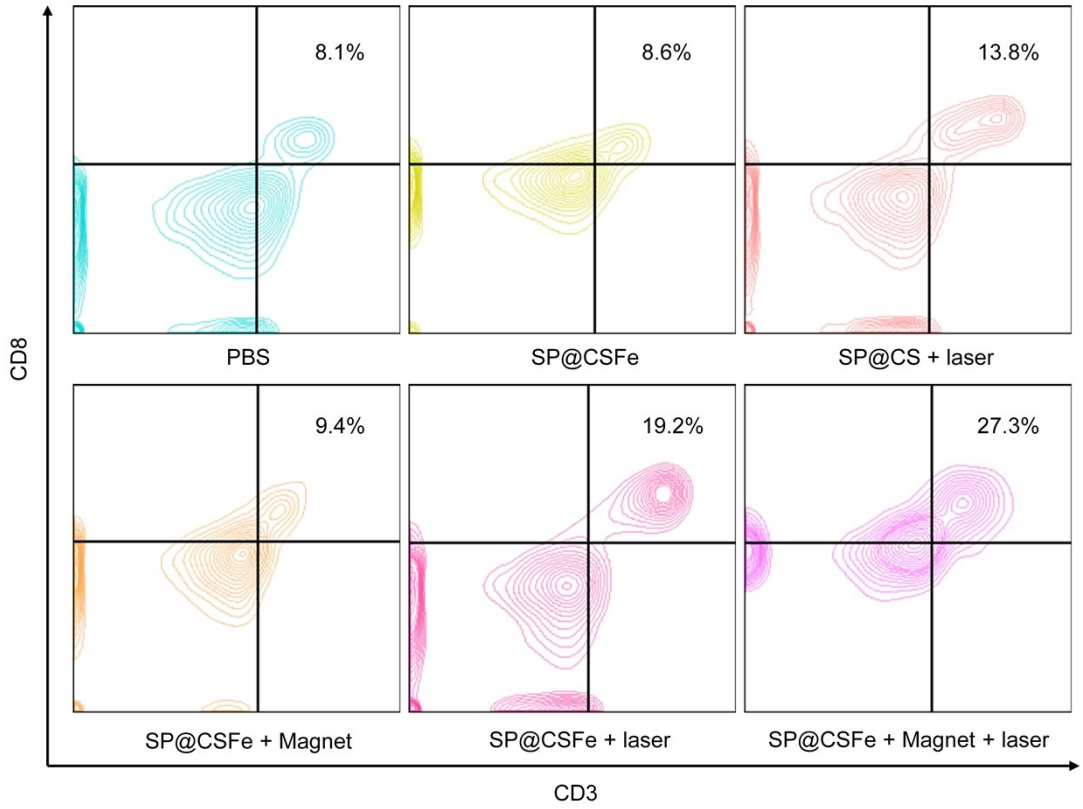

Fig. S25. Representative flow cytometry plots for $CD3^+CD8^+$ T cell analysis in distant tumors.

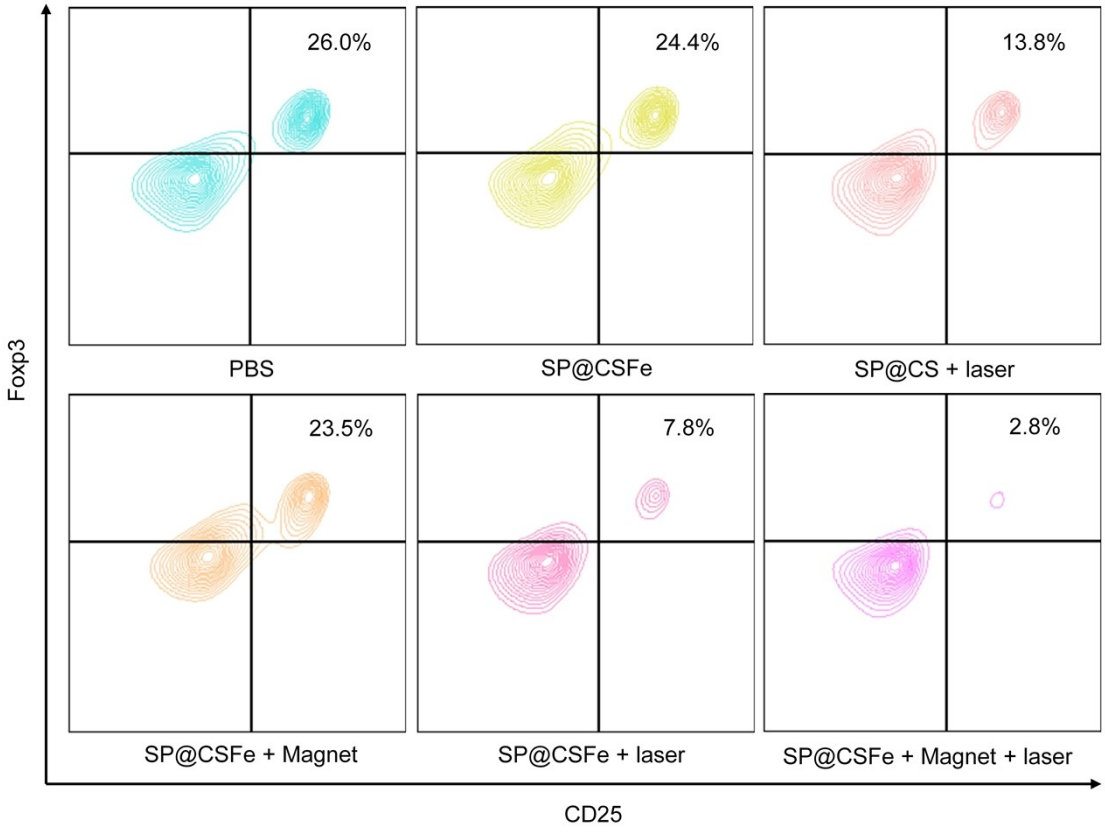

Fig. S26. Representative flow cytometry plots for T_{reg} ($CD25^+Foxp3^+$) cell analysis in distant tumors.

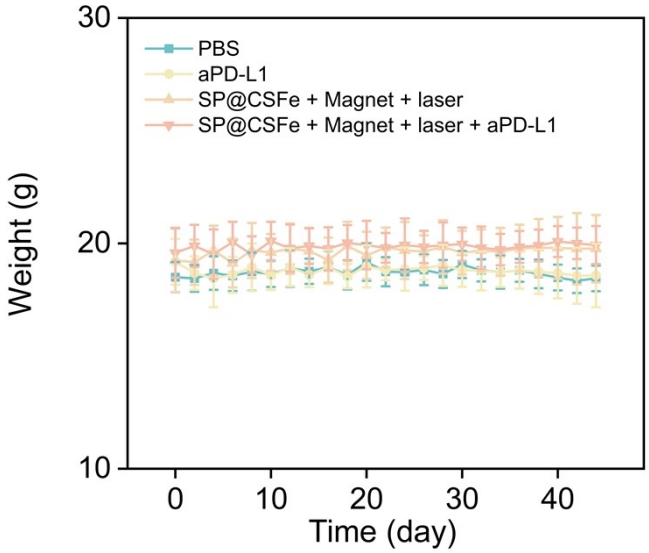

Fig. S27. Mouse body changes in the 44-day monitoring in various treatment groups (n = 5).

Experimental section

In vitro cell uptake evaluation

Cellular uptake of SP@CS and SP@CSFe was assessed in 4T1 cells by confocal laser scanning microscopy (CLSM) and flow cytometry (FCM). The cells were plated in 6-well plates and incubated with SP@CS or SP@CSFe (PCPDTBT concentration: 25 μg/mL) for 12 h. The cells were observed under a confocal fluorescence microscope, and analyzed the fluorescence intensities with ImageJ software. In parallel, the treated cells were detached, and used a 70 μm cell strainer for filtration, followed by flow cytometric analysis.

In vitro cytotoxicity evaluation

The cytotoxicity of SP@CS and SP@CSFe against 4T1 cancer cells was assessed via a cell counting kit-8 (CCK-8) viability assay. The cells were plated in 96-well plates (1×10^4 cells/well) and cultured for 24 h in complete RPMI-1640 medium. After the medium was refreshed with serial concentrations of SP@CS or SP@CSFe, incubation continued for another 24 h. Following treatment and subsequent

addition of CCK-8 solution, the plates were incubated and then read at 450 nm on a microplate reader.

In vitro therapeutic efficacy evaluation

The therapeutic efficacy of SP@CS and SP@CSFe were evaluated in 4T1 cells using a CCK-8 viability assay. The cells were plated in 96-well plates (1×10^4 cells/well) and divided into six experimental groups. These groups were received with PBS, SP@CS or SP@CSFe (PCPDTBT concentration: 25 μg/mL) for 12 h, either treated with 100 μM H2O2 or left untreated. After treatment, the cells were irradiated with 808 nm laser (1.0 W/cm^2, 5 min). Following subsequent addition of CCK-8 solution, the plates were incubated and then read on a microplate reader at 450 nm.

Characteristic morphological features of pyroptosis observation

4T1 cells were incubated for 24 h after plating in 6-well plates. The cells were treated for 6 h with fresh medium containing PBS, SP@CS or SP@CSFe (PCPDTBT concentration: 25 μg/mL). After incubation, the cells were washed with PBS and exposed to 808 nm laser irradiation (1.0 W/cm^2, 5 min). Following irradiation, the cells were then cultured in fresh medium for another 30 min. Pyroptosis-specific morphological changes were visualized and recorded using an optical microscope.

The intracellular ROS production evaluation

4T1 cells were treated for 6 h with medium containing PBS, SP@CS or SP@CSFe (PCPDTBT concentration: 25 μg/mL). The cells were treated with 10 μM H2DCFH-DA in RMPI-1640 for 30 min. After washing to remove excess probe, photothermal treatment of the cells were irradiated with 808 nm laser (1.0 W/cm^2, 5 min). Real-time imaging of intracellular ROS was conducted with a fluorescence microscope.